

Julia Mikhal

Multiscale Modeling and Simulation
Department of Applied Mathematics
University of Twente
Postbus 217
7500 AE Enschede
j.mikhal@ewi.utwente.nl

Bernard Geurts

Multiscale Modeling and Simulation
Department of Applied Mathematics
University of Twente
Postbus 217
7500 AE Enschede
b.j.geurts@utwente.nl

Research

Bounding solutions for cerebral aneurysms

Cerebral aneurysms are weak spots in the vessel structure of the brain, which present a serious problem to the patient. Julia Mikhal and Bernard Geurts present the application of an Immersed Boundary (IB) method to the simulation of blood flow through such aneurysms. The goal is to understand the flow in these diseased parts of the human brain system and to assess the risk of rupture. The IB method is applied to a generic model aneurysm for which the authors study the flow and forces on the vessel wall at a variety of physiological conditions. The definition of complex aneurysm geometries is hampered by uncertainties associated with the available spatial resolution of medical images. With the IB method one may readily approximate flow dynamics for the ‘most likely’ reference vessel shape as well as for ‘nearby’ bounding geometries. The latter approximations are respectively ‘inner’ or ‘outer’ with respect to the likely reference geometry. Several important characteristics of the flow inside the reference geometry appear to be bounded by the solutions corresponding to the inner and outer geometries. Although no strict mathematical bounding property has been established, numerical experimentation shows the practical bounding property of inner and outer simulations. The authors illustrate their numerical method on the selected ‘model aneurysm’ and show the sensitivity of the solution to inherent variations in the definition of the flow domain and flow conditions. Julia Mikhal was the winner of the Philips Wiskundeprijs voor Promovendi 2011.

Cerebral aneurysms may form and gradually develop on blood vessels in a human brain. The main risk area is the so-called ‘circle of Willis’ — the primary net of vessels through which blood is delivered to the brain. The most common locations for aneurysms to appear are near bifurcations of vessels [1]. Over time the vessel wall may be weakened and additional cavities may form, stimulated by the

ongoing pulsatility of blood flow. There are two principal methods of treatment: (i) surgical clipping near the ‘neck’ of the aneurysm, and (ii) filling the aneurysm cavity with a coiled metal wire. A main challenge is to balance the developing risk of aneurysm rupture with the risk of complications due to the surgical intervention. The coiling procedure is less intrusive and less risky than the clipping

approach, although also during insertion of a coil considerable additional forces act on the aneurysm wall that may provoke rupture [7]. Understanding and quantifying the risk of rupture may help with the planning of surgical intervention: in some cases it is better not to start surgery in view of these additional complications. Computational modeling can be an important support in the treatment — in this paper we sketch the use of an immersed boundary method to obtain flow and forces from a computer simulation, and consequently arrive at a basic ingredient for future risk modeling.

These days, the diagnostics of cerebral aneurysms is based on a rotational angiography procedure during which 2D and 3D images of the often complex vessel structure are determined [3, 9]. Based on impressions of, e.g., size, shape and location of possible aneurysms, medical decisions are made regarding further treatment. Considerable heuristics and a large volume of circumstantial knowledge is implicitly embedded in such decision processes. Through numerical simulation of flow patterns inside actual vessel structures one may augment the current

mode of operation by patient-specific prediction of forces on the aneurysm walls. In this paper we illustrate how an immersed boundary method can be used, not only to predict the flow dynamics, but also to provide an impression of upper and lower bounds for a range of key flow properties. This can be used to quantify the sensitivity of the predictions to input uncertainties, but also suggests savings in the computational effort by bounding flow properties with inner and outer predictions obtained at rather coarse spatial resolutions.

The flow of blood is modeled by approximating it as a Newtonian fluid, i.e., governed by the incompressible Navier–Stokes equations. The dynamic consequences of non-Newtonian corrections were found to be quite small [2, 5, 10]. The flow is predicted on the basis of an immersed boundary method [8]. Basic to this approach is the so-called binary ‘masking function’ H with which the complex geometries of (diseased) human blood vessels is represented. In fact, we specify the geometry by identifying which locations are inside a solid part ($H = 1$) of the domain and which are in a fluid part ($H = 0$). The pattern of 0’s and 1’s on a given spatial grid provides a ‘staircase’ approximation of the vessel geometry, and allows to numerically simulate the flow, consistent with the impenetrability of the solid brain tissue. The use of a masking function yields a fast and simple definition of patient-specific geometries that were obtained from an angiography procedure. Moreover, slight uncertainty in the precise location of the boundary between the solid ($H = 1$) and the fluid ($H = 0$) part of a recorded angiography can be accommodated for. In the sequel, we will sketch the numerical method, present the prediction of flow and forces in a model aneurysm and describe the use of inner and outer masking functions to provide practical bounds for various flow characteristics.

Immersed Boundary method

We simulate the flow of blood inside the human brain by solving the incompressible Navier–Stokes equations:

$$\frac{\partial \mathbf{u}}{\partial t} + \mathbf{u} \cdot \nabla \mathbf{u} = -\nabla p + \frac{1}{\text{Re}} \nabla^2 \mathbf{u} + \mathbf{f}, \quad (1)$$

$$\nabla \cdot \mathbf{u} = 0, \quad (2)$$

$$\text{with } \mathbf{u} = \mathbf{0} \text{ at } \partial\Omega_f. \quad (3)$$

Here \mathbf{u} is the velocity of the fluid in the flow domain Ω_f , p is the pressure and $\text{Re} = UL/\nu$ is the Reynolds number, in terms of a refer-

ence velocity (U), a reference length scale (L) and the kinematic viscosity (ν). In this paper the length scale is of the order of the diameter of a vessel connecting to an aneurysm, while the reference velocity is of the order of the bulk velocity derived from the mass flow rate Q and the cross-sectional area of a vessel A , i.e., $U = Q/A$.

The non-dimensional parameter Re is interpreted here as a measure for the speed of the blood flow, assuming the viscosity and the length scale parameter to be fixed. To appreciate the flow regime, e.g., laminar or turbulent flow, it is important to estimate the value of Re . In the circle of Willis a typical diameter of a vessel is $D \approx 0.42 \pm 0.09$ cm [6]. The kinematic viscosity is on the order of $\nu \approx 3.5 \cdot 10^{-6}$ m²/s [12]. Finally, a typical mass flow rate $Q \approx 245$ ml/min [4], which implies a velocity $U \approx 0.3$ m/s. These numbers lead to a Reynolds number $\text{Re} \approx 350$. Since the Reynolds number can vary considerably from person to person, depending on a number of aspects such as the level of activity at a given time, the precise vasculature that is present or the actual viscosity of the blood, we will consider the physiologically relevant range $\text{Re} = 100$ – 500 in the computations. This corresponds to a laminar, possibly unsteady flow regime. We discretize the system of Navier–Stokes equations by adopting a symmetry-preserving finite volume method in combination with a time-stepping method of Adams–Bashforth type [13].

The forcing term \mathbf{f} on the right hand side of the Navier–Stokes equations is used to represent the condition that brain tissue can not be penetrated by the flow. This condition can be represented in various ways. In the current immersed boundary approach we adopt a volume penalization that depends linearly on the flow velocity \mathbf{u} . In particular, we select the forcing in the following way:

$$\mathbf{f} = -\frac{1}{\varepsilon} H(\mathbf{x}) \mathbf{u}.$$

Here H is the so-called masking function and the ‘relaxation time’ $\varepsilon \ll 1$. The masking function H is a binary function that takes the value ‘0’ if \mathbf{x} is in the fluid-filled part of the physical domain and the value ‘1’ for all \mathbf{x} in the solid part (see Figure 1). The linear forcing term induces a very strong restoring influence on any non-zero flow inside the solid brain tissue. This results in negligible velocities where $H = 1$; we adopt $\varepsilon = 10^{-10}$ and observed maximal residual velocity values in the solid on the order of $\sqrt{\varepsilon}$. Hence, the volume

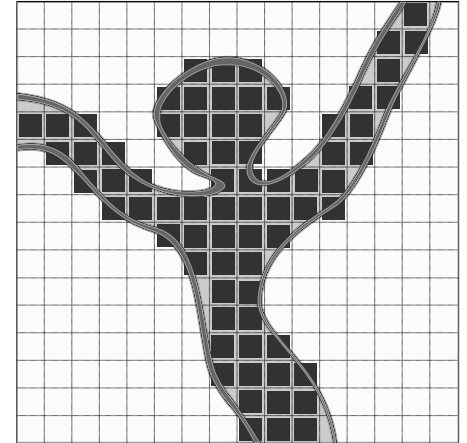


Figure 1 Sketch of the masking function in 2D. The fluid cells (dark) are assigned according to the domain property in the centre of the grid cell — if the center is found to be solid (fluid) then the entire cell is assigned to be solid (fluid).

penalization is effective in retaining the incompressible Navier–Stokes equations within the flow part of the physical domain, while yielding effectively zero velocity within the solid part.

Within our IB method we work on a 3D Cartesian grid, which simplifies computations, but also makes the treatment of arbitrary complex geometries a challenging problem. In general, a complex shape will not be aligned with the regular Cartesian grid, and some approximations need to be made. Turning this challenging aspect into a ‘virtue’ of the method, we developed three closely related masking function techniques, which allows not only to predict the numerical solution but also its sensitivity to small uncertainties in the geometry definition. The three masking strategies are referred to as ‘inner’, ‘middle’ and ‘outer’; these differ in the way a value of H is assigned to a grid cell. In the ‘middle’ strategy we call a grid cell solid (fluid) if the centre of the cell is solid (fluid). For the ‘inner’ strategy we are more strict and call a grid cell part of the fluid domain if *all* eight corner points of that cell are in the fluid part. Similarly, in the ‘outer’ strategy a grid cell is assigned to be part of the fluid domain if at least two of the eight corner points of the grid cell are in the fluid part. Correspondingly, the flow domain associated with the ‘inner’ (‘outer’) strategy will be smaller (larger) than that corresponding to the ‘middle’ strategy, a property that is basic to deriving practical numerical bounding solutions, as will be shown in the sequel. We validated these strategies for the classical case of Poiseuille flow through a cylindrical pipe and obtained first order convergence for a basic discretization method (see Figure 2). This illustrates the

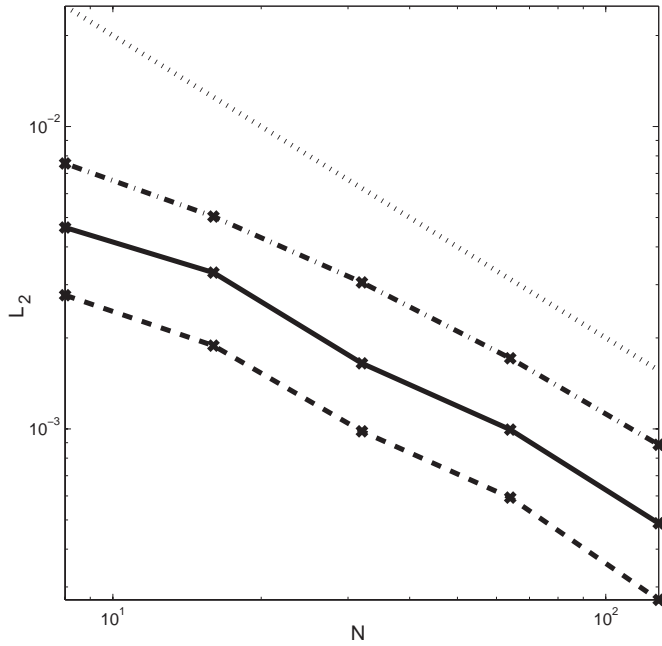


Figure 2 Convergence of the error computed in the L_2 norm for inner (dash), outer (dash-dot) and middle (solid) masking strategies, applied to Poiseuille flow in a cylindrical pipe. The validation analysis includes several grid resolutions. For convenience a slope of -1 is included (dot) to help appreciate the first order convergence at high resolutions.

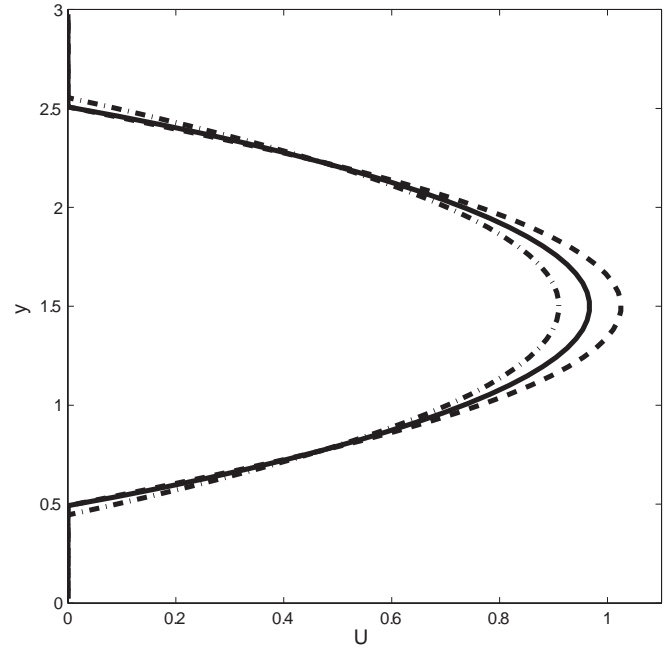


Figure 3 The velocity profiles for inner (dash) and outer (dash-dot) masking functions bound the middle profile (solid). The grid resolution is 64×64 over the cross section of the cylinder.

consequence of non-alignment of the fluid-solid interface with the Cartesian grid. Next to the numerical convergence of our method we notice that several aspects of the ‘middle solution’ are nicely bounded by the solutions obtained with the ‘inner’ and ‘outer’ masking strategies. In Figure 3 the parabolic

Poiseuille profile obtained for the middle solution is bounded from above and below by the inner and outer solutions.

The three definitions of the masking function can be used to investigate the sensitivity of flow predictions to the quality with which the geometry is known. From medical

imagery the geometry of blood vessels is available with a certain limited spatial resolution — pivoting about what we believe to be the more probable approximation of the shape of the aneurysm, can give a confidence level to the numerical findings. The inner and outer strate-

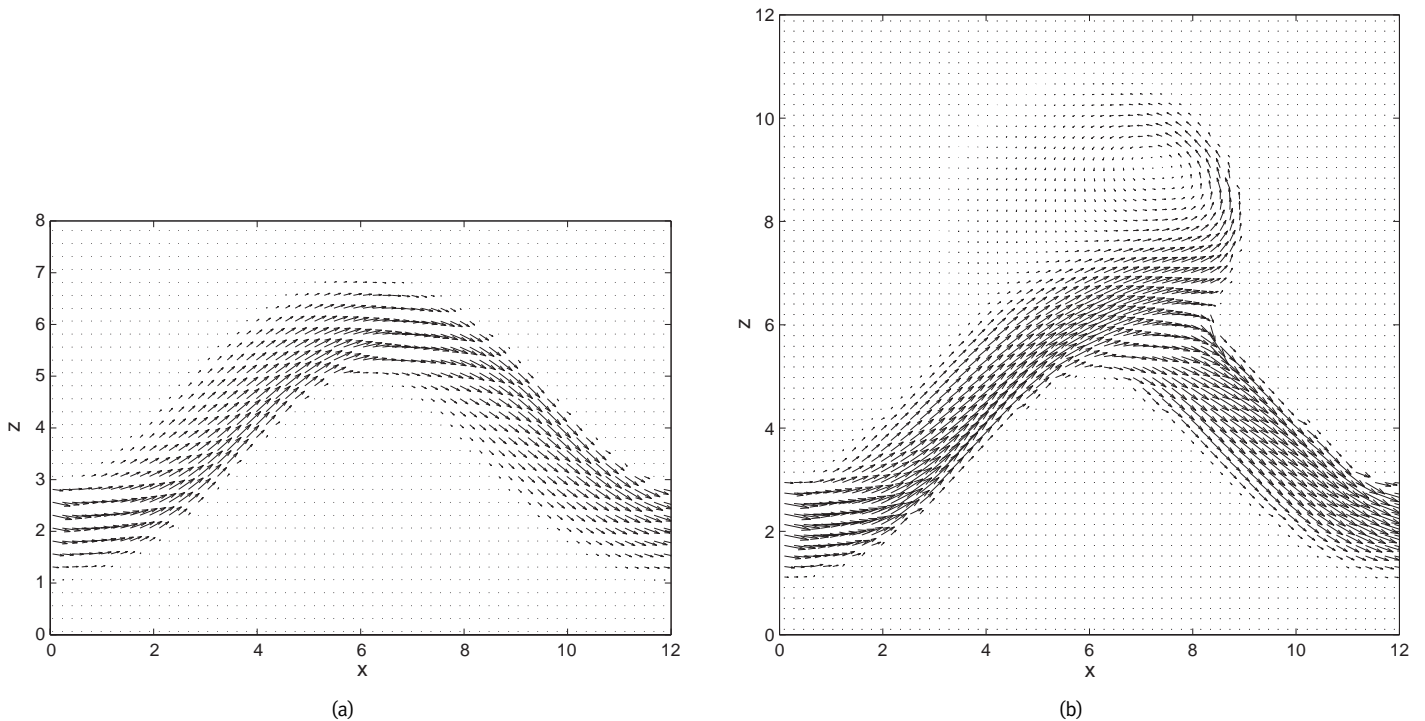


Figure 4 Snapshot of the developing flow inside a curved vessel (a) and a model aneurysm (b) at $Re = 100$. The flow is visualized in a cross-section through the geometry, by plotting the in-plane velocity vectors.

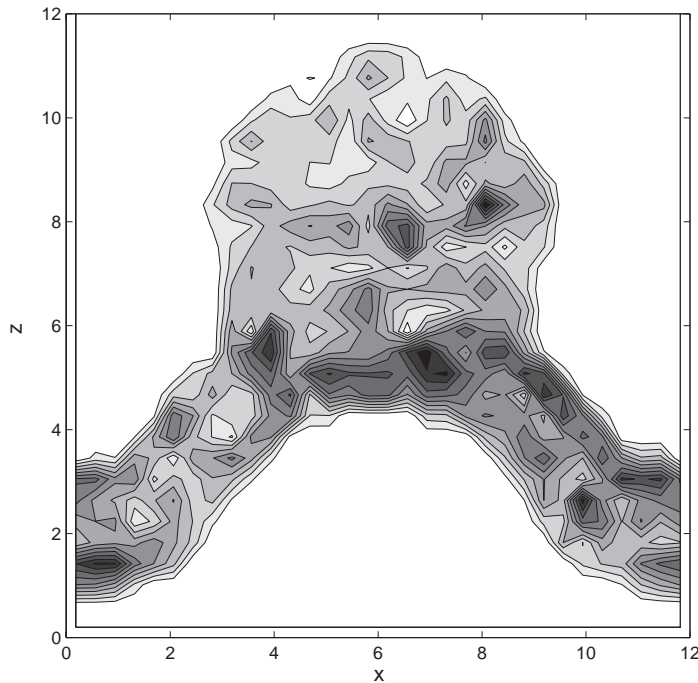


Figure 5 Snapshot of the shear stress distribution in a 2D cross section through the middle of the model aneurysm. Simulations are done for a pulsatile flow at $Re = 500$. Dark areas correspond to high shear stress values.

gies can provide such practical bounds, which can be used for better understanding of the natural uncertainties.

Shear stress and forces on vessel walls

Analysing images of real aneurysms from

patient data motivates to first develop the IB method on the basis of characteristic ‘building-block’ shapes for connecting vessels and aneurysm bulges. We selected a model curved vessel formed by a cylindrical tube with a sinusoidal centre-line. By adding a

spherical cavity to this curved vessel we arrive at the definition of a model aneurysm.

An impression of the flow through these two models is shown in Figure 4. We observe a well-defined flow through the curved vessel, which becomes more complex by the presence of vortex shedding in the aneurysm cavity. Although there is a direct interest in the evolution of the actual flow, an assessment of the possible ‘risk of rupture’ of such a flow configuration requires also knowledge of the forces that act on the walls. To quantify these, it is common practice in fluid mechanics to determine the so-called shear stress τ , which is a measure for the gradient of the velocity field in the flow domain [11]. Defining the rate-of-strain tensor $S = (\nabla \mathbf{u} + (\nabla \mathbf{u})^T)/2$ in terms of the velocity gradient $\nabla \mathbf{u}$ we compute

$$\tau = \frac{1}{Re} \sqrt{2S : S}$$

The shear stress helps us to analyse the shear forces in the whole computational domain. To isolate normal stresses from pure shearing motion we base τ on the off-diagonal components of S . A 2D impression of the shear stress distribution taken in a slice through the middle of the model aneurysm can be found in Figure 5. We show contours of τ at a characteristic moment during the time-dependent flow — dark areas correspond to high shear stress, which are mostly located along the

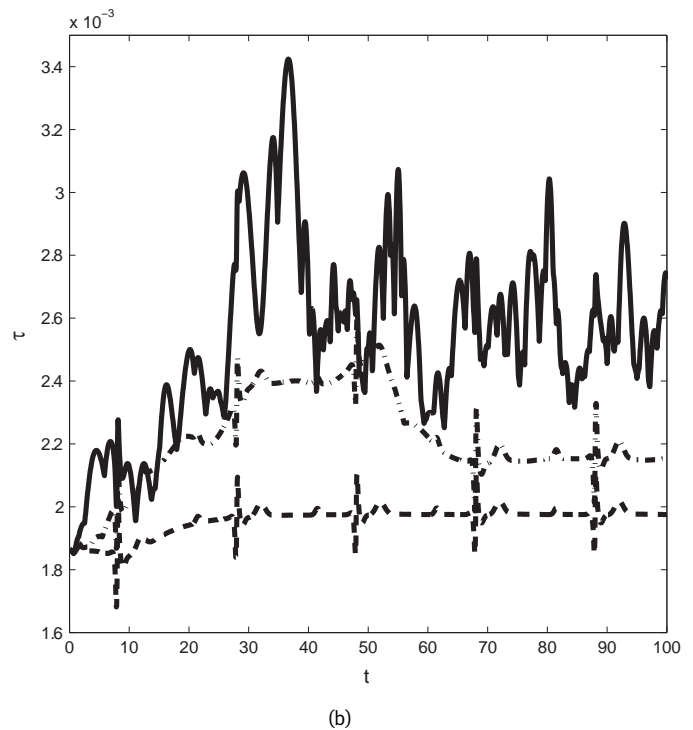
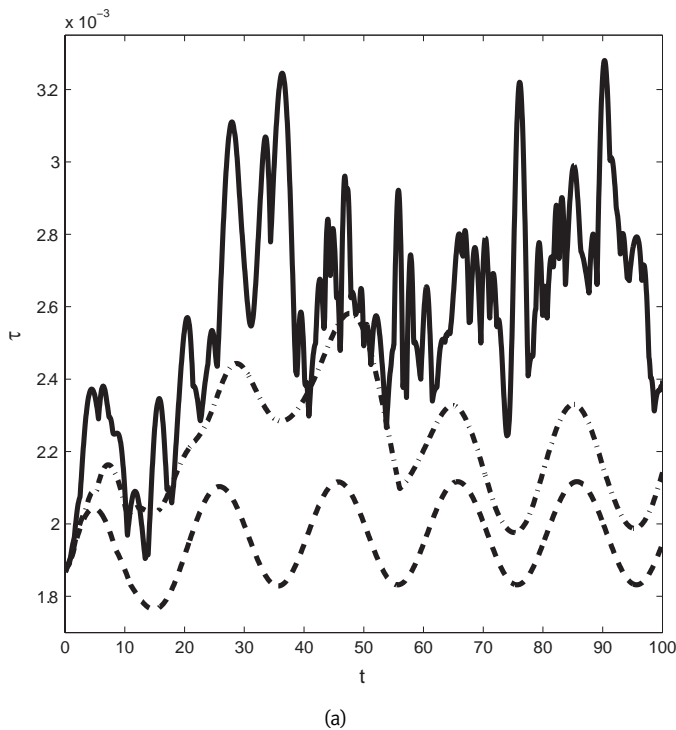


Figure 6 The maximum shear stress inside the model aneurysm for pulsatile flow forced by a sinusoidal (a) and a realistic cardiac (b) mass-flow forcing. The flow was simulated at different physiologically relevant Reynolds numbers: $Re = 100$ (dash), $Re = 250$ (dash-dot) and $Re = 500$ (solid). At lower Reynolds numbers the selected pulsatile profile is clearly visible in the shear stress response, while for higher Reynolds numbers the nonlinearity of the flow is dominant and the response becomes largely independent of the forcing profile.

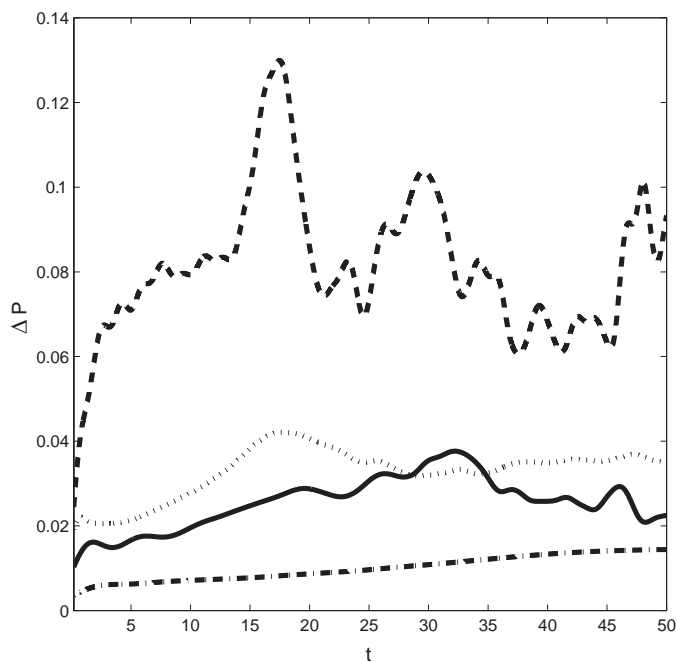


Figure 7 Pressure drop in the streamwise direction over the model aneurysm for inner (dash), middle (solid) and outer (dash-dot) solutions at a coarse grid resolution $32 \times 16 \times 32$, and the middle (dot) solution obtained at a higher grid resolution $64 \times 32 \times 64$. Simulations are done at $Re = 500$.

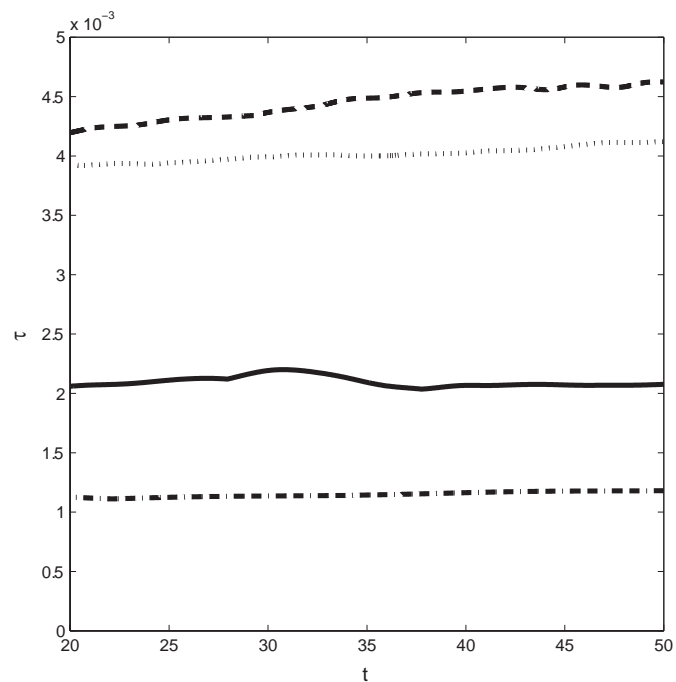


Figure 8 Time-averaged maximum shear stress over the model aneurysm for inner (dash), middle (solid) and outer (dash-dot) solutions at a coarse grid resolution $32 \times 16 \times 32$, and the middle (dot) solution obtained at a higher grid resolution $64 \times 32 \times 64$. Simulations are done at $Re = 500$.

walls, near the neck of the aneurysm and associated with localized swirling motion (vortices) inside the aneurysm.

A focus of interest is the effect of pulsatile flow on the shear stresses inside the model aneurysm. For this purpose we force the flow by a time-periodic pressure drop across the streamwise direction, such that a time-dependent mass flow arises. We consider two types of pulsatile signals: a simple sinusoidal signal and a signal approximating a realistic cardiac cycle. We compute the maximum of the shear stress over the flow domain as a function of time.

In Figure 6 we present the computational results at three flow conditions in the physiologically relevant regime, i.e., at $Re = 100$, $Re = 250$ and $Re = 500$. At lower Reynolds numbers, i.e., at comparably slow flow in case we consider the domain size and the viscosity of blood fixed, the pulsatile forcing profile is clearly visible in the time-dependent response. At higher Reynolds numbers the non-linearity of the Navier–Stokes equations is dominant over the precise forcing effects and the response is largely independent of the selected mass-flow profile. In addition, we observe a considerable growth in the maximal shear stress levels, with increasing flow velocity. The combination of a strongly fluctuating stress level, with considerably increased amplitude corresponds intuitively with an in-

crease in the risk of rupture at higher Re — current research is dedicated to capturing these trends in a quantitative risk model.

Inner/outer bounding solutions

In this section we illustrate the practical bounding solutions obtained on the basis of the ‘inner’ and ‘outer’ masking functions. We concentrate on analysing the pressure drop over and the stress level in the model aneurysm. In order to maintain a prescribed mass-flow through the computational domain a time-dependent pressure difference needs to be provided. In Figure 7 we present this pressure drop as obtained for the three masking strategies. We also present the time-averaged maximum shear stress in Figure 8. The numerical results show the practical bounding property associated with the inner and outer masking functions, relative to the findings based on the ‘most probable’ middle masking function. At coarse grids, the predictions obtained with ‘nearby’ masking functions can be qualitatively different, emphasizing the need to quantify the sensitivity of any flow prediction to changes in the aneurysm geometry. Even at the coarse spatial resolutions that were adopted in these illustrations, we notice that the pressure drop and shear stress measure found with the middle masking function are bounded from below and above by the inner and outer results at

the same grid resolution. When increasing the spatial resolution, the practical bounding property is maintained and the band-width within which the predictions are likely to fall decreases.

In Figures 7 and 8 we also included predictions obtained at higher resolutions. These suggest a possible further usage of the practical bounding idea: instead of one expensive computation at high resolution for the ‘middle’ geometry we can provide bounding predictions at considerably lower grid resolutions. In some cases such coarse bounding of a certain flow property may be adequate, thereby avoiding the need for grid refinement. Such an approach could bring realistic on-line computation during surgical procedures much closer. Since there is no strict mathematical proof given for the observed bounding property, the practical usage of this idea is subject to numerical experimentation to obtain confidence in the results.

Conclusions

We presented a numerical model for the simulation of blood flow inside a cerebral aneurysm. The risk of rupture of such an aneurysm is connected to the time-dependent forces acting on the wall of the aneurysm. The long-term development of an aneurysm constitutes an important multiscale problem where ‘expected’ develop-

ments that take place over tens of millions of heart beats need to be assessed on the basis of the dominant structures in a pulsatile flow on the scale of a second. Robustness of predictions is then of utmost importance. In this paper we focused on the sensitivity of flow

mechanics predictions arising from uncertainties in the basic medical imagery that is available. For the definition of the vessel geometry we proposed to use inner/middle/outer masking strategies, yielding instead of one solution for a 'most probable' aneurysm ge-

ometry an interval of values where the fully resolved solution is expected to lie. With the use of the bounding solutions we can more reliably present the results and express the sensitivity of flow and forces to the definition of the geometry. ←

References

- 1 G. N. Foutarakis, H. Yonas and R. J. Scلابassi, 'Saccular Aneurysm Formation in Curved and Bifurcating Arteries', *AJNR Am J. Neuroradiol.*, 20, pp. 1309–1317, 1999.
- 2 F. J. H. Gijsen, F. N. Van de Vosse and J. D. Janssen, 'The Influence of the Non-Newtonian Properties of Blood on the Flow in Large Arteries: Steady Flow in a Carotid Bifurcation Model', *Journal of Biomechanics*, 32, pp. 601–608, 1999.
- 3 M. Grass, R. Koppe, E. Klotz, R. Proksa, M. H. Kuhn, H. Aerts, J. Op de Beek and R. Kemkers, 'Three-dimensional Reconstruction of High Contrast Objects Using C-arm Image Intensifier Projection Data', *Computerized Medical Imaging and Graphics*, 23, pp. 311–321, 1999.
- 4 J. Hendrikse, A. F. van Raamt, Y. van der Graaf, W. P. T. M. Mali and J. van der Grond, 'Distribution of Cerebral Blood Flow in the Circle of Willis', *Radiology*, 235, pp. 184–189, 2005.
- 5 J. Janela, A. Moura and A. Sequeira, 'A 3D Non-Newtonian Fluid-Structure Interaction Model for Blood Flow in Arteries', *Journal of Computational and Applied Mathematics*, 234, pp. 2783–2791, 2010.
- 6 S. Kamath, 'Observations on the Length and Diameter of Vessels Forming the Circle of Willis', *J. Anat.*, 133, pp. 419–423, 1981.
- 7 E. Lusseveld, E. H. Brilstra, P. C. G. Nijssen, W. J. J. van Rooij, M. Sluzewski, C. A. F. Tulleken, D. Wijnalda, R. L. L. A. Schellens, Y. van der Graaf and G. J. E. Rinkel, 'Endovascular Coiling versus Neurosurgical Clipping in Patients with a Ruptured Basilar Tip Aneurysm', *J. Neurol. Neurosurg. Psychiatry*, 73, pp. 591–593, 2002.
- 8 R. Mittal and G. Iaccarino, 'Immersed Boundary Methods', *Annu. Rev. Fluid Mech.*, 37, pp. 239–261, 2005.
- 9 J. Moret, R. Kemkers, J. Op de Beek, R. Koppe, E. Klotz and M. Grass, '3D Rotational Angiography: Clinical Value in Endovascular Treatment', *Medicamundi*, 42-3, pp. 8–14, 1998.
- 10 K. Perktold, R. Peter and M. Resch, 'Pulsatile Non-Newtonian Blood Flow Simulation Through a Bifurcation with an Aneurysm', *Biorheology* 26(6), pp. 1011–1030, 1989.
- 11 S. B. Pope, *Turbulent Flows*, Cambridge University Press, 2003.
- 12 A. Quarteroni and L. Formaggia, *Mathematical Modelling and Numerical Simulation of the Cardiovascular System, Handbook of Numerical Analysis*, Editors P. G. Ciarlet and J. L. Lions. North-Holland Vol. XII, pp. 3–127, 2004.
- 13 R. W. C. P. Verstappen and A. E. P. Veldman, 'Symmetry-Preserving Discretization of Turbulent Flow', *J. Comput. Phys.*, 187, pp. 343–368, 2003.